Mussel-inspired Self-healing Coatings Based on Polydopamine Coated Nanocontainers for Corrosion Protection

Bei Qian[1, 2], Zhaoliang Zheng[2], Marios Michailids[2], Nicole Fleck[2], Matthew Bilton[3], Yan Song[4], Guoliang Li[4], Dmitry Shchukin[2,5]*

[1]College of Chemistry and Pharmaceutical Sciences, Qingdao Agricultural University, 700 Changcheng Road, Qingdao 266109, PR China.

[2]Stephenson Institute for Renewable Energy, Department of Chemistry, University of Liverpool, Crown Street, Liverpool L69 7ZD, U.K.

[3]Imaging Centre at Liverpool, University of Liverpool, Liverpool L69 3GL, U.K.

[4]Institute of Process Engineering, Chinese Academy of Sciences, Beijing 100190, PR China.

[5]Northwestern Polytechnical University, Xi'An, 710072, PR China.

KEYWORDS: Silica; dopamine; self-healing; mild steel; corrosion protection

ABSTRACT: Mussel-inspired properties of dopamine have attracted immense scientific interest for surface modification of nanoparticles due to the high potential of dopamine functional groups to increase adhesion of nanoparticles to flat surfaces. Here, we report for the

first time a novel type of inhibitor-loaded nanocontainers using polydopamine (PDA) as a pH-sensitive gatekeeper for mesoporous silica nanoparticles (MSNs). The encapsulated inhibitor (benzotriazole) was loaded into MSNs at neutral pH, demonstrating fast release in acidic environment. Self-healing effect of water-borne alkyd coatings doped with nanocontainers was achieved by both on-demand release of benzotriazole during the corrosion process and formation of the complexes between the dopamine functional groups and iron oxides thus providing dual self-healing protection for the mild steel substrate. The coatings were characterized by Electrochemical Impedance spectroscopy, visual observations and confocal Raman microscopy. In all cases, the coatings with embedded benzotriazole-loaded MSNs with PDA-decorated outer surface demonstrated superior self-healing effect on the damaged areas. We anticipate that dopamine-based multifunctional gatekeepers can find application potential not only in intelligent self-healing anticorrosive coatings but also in drug delivery, antimicrobial protection and other fields.

INTRODUCTION

Corrosion mostly affects the petroleum, cement and concrete manufacturing industries, metal processing, water treatment, chemical processing and power generation equipment. In recent years there has been a considerable increase in the global anticorrosion coatings' market. According to a 2018 report from Bcc Research (https://www.bccresearch.com/) it should reach $31.0 billion by 2022, up from $23.3 billion in 2017. According to the technical classification, the market for anticorrosion coatings can be divided into solvent-borne, water-borne, powder-based, self-healing and other paint formulations. Water-borne coatings gained a significant increase of the market share over the past decades owing to strong regulations related to volatile organic compound (VOC) emissions from solvent-borne coatings. Addition of self-healing components will attain to the water-borne coatings the internal capability to repair corrosion

damage by themselves (autonomic) or with the help of outside triggers such as light, heat or mechanic pressure, which is highly desirable for novel coating products.[1-3]

Usually, self-healing coating is impregnated with nanocontainers or microcapsules, which encapsulate inhibitors or healing agents.[4-5] Mesoporous silica nanoparticles (MSNs) are ideal nanocontainers because both their size and pore volume are easily controlled to optimize inhibitor encapsulation process.[6-9] However, the application of MSNs as delivery tools in self-healing coatings is limited by spontaneous leakage of small molecular inhibitors from mesopores.[8] Bioinspired nanovalves prepared from metal precipitates and supramolecular materials have been proven to be applicable gatekeeper for the nanocontainers.[10-15] Besides the high cost, the major drawback of these nanovalves is their single function, which only serves as the pH-controlled release gatekeeper. It would be important for MSNs' gatekeeper to have additional functionality of the pH-controlled release effect. To the best of our knowledge, multifunctional gatekeepers for controlled release have been scarcely reported up to now in literature.[16]

Inspired by the adhesive nature of catechols and amines in mussel adhesive proteins, polydopamine (PDA) is one of the most versatile approaches for functionalizing almost all nanomaterial surfaces.[17-18] The coating with PDA can be formed in the alkaline pH solution without any external stimuli such as light or heat, and its uniformity depends on the PDA diffusion and surface reactivity. Recently, the PDA coated MSNs have been shown as pH-sensitive release system for drug delivery.[19-20] It is noteworthy that the unreacted catechol groups after the oxidative polymerization of dopamine could leave abundant hydroxyl groups on the surface of MSNs, which endow the decorated nanocontainers increased wettability. This property is crucial for nanocontainers dispersed in water-borne coatings. Moreover, catechol groups have another outstanding function for self-healing coatings. It is reported that the cracked polymer networks can be reconnected by catechol-Fe^{3+} coordinate bonds.[21] Another

paper reported that the cation-π interaction modulated by salt is a key mechanism in the mussel adhesion process.[22] All these findings aroused our great interest to apply PDA as the pH-release gatekeeper for the inhibitor loaded MSNs. Although many researchers have directly applied PDA into the coatings or on the metal surfaces for corrosion protection,[23-31] there is no evidences of using PDA as a gatekeeper in smart mesoporous nanocontainers. Besides the pH release control property, we want to explore other PDA functionalities for the anticorrosion self-healing coatings.

In this study, we designed a mussel-inspired self-healing coating by application of MCM-48 MSNs as nanocontainers for benzotriazole (BTA), a well-known inhibitor of steel corrosion.[32-35] MCM-48 was chosen because of its branched internal 3D mesostructure.[36-38] It was used as nanoreservoirs for biocides in our previous work.[39] The next step was functionalization of BTA-loaded MSNs with PDA layer. Hence, we report here a novel design of PDA-decorated MSNs nanocontainers for self-healing coatings. We believe that our work will stimulate other researchers to explore more multifunctional gatekeepers for self-healing and other applications.

EXPERIMENTAL METHODS

Materials.

Tetraethyl orthosilicate (TEOS, 98%), hexadecyltrimethylammonium bromide (CTAB, 99%), triblock copolymer F127 (Pluronic F127), ammonium hydroxide (32%), ethanol (99.8%), 1H-benzotriazole, hydrochloride dopamine and tris (hydroxymethyl) aminomethane (Tris) were purchased from Sigma-Aldrich, UK. The investigated mild steel was supplied by Metal Store, UK.

Synthesis of MSNs.

MSNs were synthesized according to the method reported by Kim et al.[36] CTAB (0.5 g) and Pluronic F127 (2.05 g) were dissolved in a mixture of deionized water (96 mL) and pure ethanol

(43 mL), and ammonium hydroxide (11 mL of 32 wt% solution) was then added to the solution. The solution was stirred for 40 min at 600 rpm to dissolve the solid completely. On the next step, TEOS (1.8 g) was added into the mixture at once. After stirring at 1000 rpm for 24 h at room temperature, the resulting solid was recovered by filtration, washed twice with ethanol, twice with distilled water and dried in air under ambient conditions. The organic template was removed by calcination in a muffle furnace at 550 °C for 6 h after heating up with a ramp of 1 °C/min.

BTA loading and PDA modification.

Before loading, the MSNs were dried at 120 °C under vacuum to remove water and air from the mesoporous structure. Then, 10 mg of MSNs were directly dispersed in the solution of BTA in ethanol (10 wt%, 10 mL). The mixed solution was placed in desiccator and evacuated using a vacuum pump at room temperature so BTA could be uploaded into the mesopores of the MSNs. The vacuum cycle was repeated thrice to obtain the maximum loading of inhibitor (21 wt.%). The as-loaded MSMs (MSNs-BTA) were separated by centrifugation and dried for 24 h at 323 K. The loading capacity of the BTA is about 30 wt% confirmed by thermogravimetric analysis of the MSNs-BTA, which has not been shown in this paper. It is worth mentioning that any post-treatment of the MSNs-BTA in water will lead to leakage of the loaded BTA. Washing of these nanocontainers with ethanol will lead to even faster leakage of BTA due to its high solubility in organic solvents. Ultrasonic dispersion of the MSNs-BTA will cause complete release of the inhibitor within only 1 min. To deposit a PDA layer on the surface of the loaded nanocontainers, MSNs-BTA (30 mg) was dispersed in 30 mL Tris-HCl buffer (pH 8.5) solution saturated with BTA. Then, 60 mg of hydrochloride dopamine was immediately added. The mixture was stirred for 12 h in the dark. The resulted PDA coated MSNs-BTA (MSNs-BTA@PDA) nanocontainers were separated by centrifugation (12000 rpm, 20 min) and washed with water to remove the unpolymerized dopamine.

Coating.

The water-based alkyd paint was purchased from Crown Trade, UK. MSNs-BTA@PDA (2 wt%) was added to the alkyd emulsion and mechanically stirred by a homogenizer. Paints without MSNs (blank coating), with 2 wt% MSNs and 2 wt% MSNs-BTA were prepared for comparison. The coatings were deposited on the mild steel plates using a paint applicator (RK Paint Applicator, UK) and dried at room temperature for 48 h. The wet film thickness of all studied coatings was controlled at 60 μm by paint applicator. The dry thickness of the coating is 5 ± 0.5 μm measured by profilometer (AMBios XP-200).

Characterization.

The morphology, size and pore structure of the MSNs were characterized by scanning electron microscopy (SEM, JEOL 7001F), X-ray powder diffraction (XRD, Bruker D8 Venture), nitrogen adsorption isotherms (BET, Quantachrome Instruments) and transmission electron microscopy (TEM, JEOL 2100FCs). The chemical structure of MSNs, MSNs-BTA and MSNs-BTA@PDA was determined through attenuated total reflection Fourier-transform infrared spectra (ATR-FTIR, Bruker TENSOR II, UK) in the wavenumber range from 4000 to 400 cm^{-1}. UV-vis spectroscopy (Evolution 201 UV-visible spectrophotometer, Thermo Scientific, UK) was applied to characterize the release profile of BTA. The characterization method was used according to our previous research.[10] To avoid the influence of the PDA, absorbance of BTA at 258 nm was plotted against time. Electrochemical impedance spectroscopy (EIS, Ivium CompactStat, Netherlands) measurements were used to record the corrosion behaviour of the self-healing coating. Mild steel substrates (3cm × 6cm × 0.3cm) with coatings were placed into special cells as shown in supporting information (4 cm^2 of the sample area exposed to the 0.1 M NaCl electrolyte). The electrolyte was fixed in a glass tube by an O-ring. The electrolyte inside the glass tube was renewed every 24 hours. The platinum sheet was used as the auxiliary electrode, and Ag/AgCl electrode was used as the reference electrode. Both intact and scratch

samples were tested. Scratches were made with a circular-edge scalpel by a home-made machine. The scratch area is 10 mm long, 200 μm wide, and 80 μm deep. Open circuit potential was measured for 30 min following EIS measurements with the frequency from 10^5 Hz to 10^{-2} Hz using AC signal amplitude of 10 mV. All electrochemical tests were performed three times to guarantee their repeatability and average values with error bars are demonstrated in experimental results. EIS data were fitted to equivalent cell diagrams using the IviumSoft program. The corrosion products formed on the mild steel substrates were characterized by Raman spectra (LabRam Xplora confocal Raman microscope, Horiba Jobin Yvon, France). After 20 days of immersion, the coating was removed the by knife. After the removal, the substrate was washed with acetone several times to completely remove coating residues.

RESULTS AND DISCUSSION

Characterization of MSNs, MSNs-BTA, and MSNs-BTA@PDA.

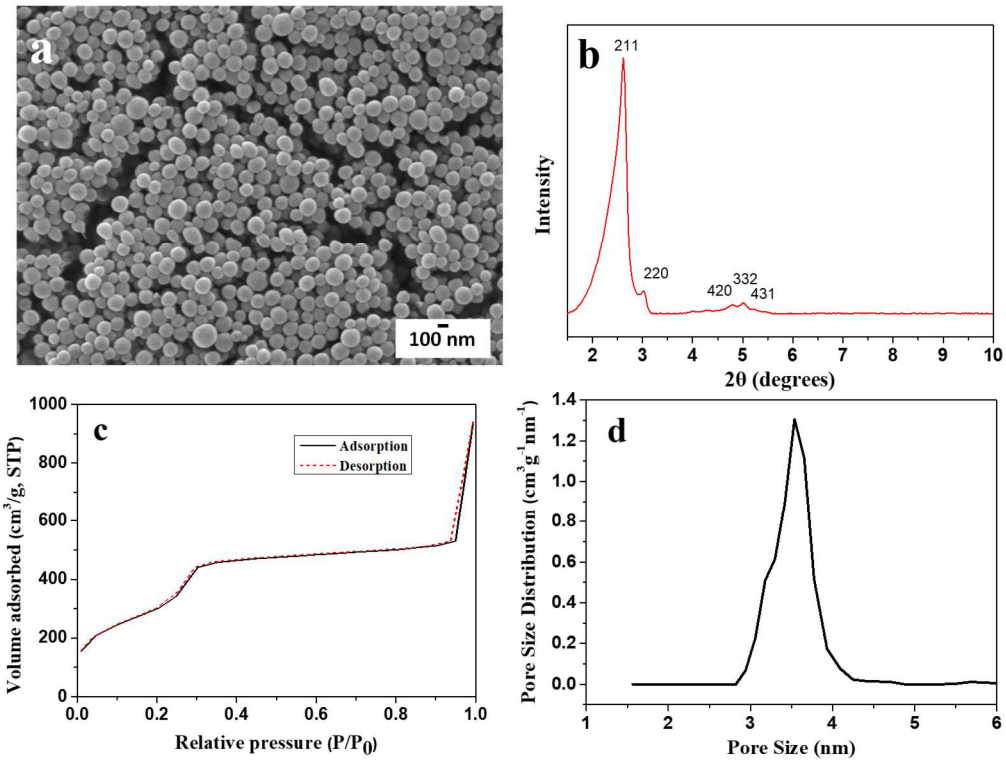

Figure 1. SEM image (a), XRD (b), N_2 sorption isotherm (c), and pore size distribution (d) of MSNs.

Fig. 1 (a) shows the SEM image of MSN. All particles exhibit spherical shape with size range between 90 nm and 170 nm. Fig. 1 (b) demonstrates the XRD pattern of MSNs. Five peaks were observed on the XRD pattern, which correspond to the planes (211), (220), (420), (332) and (431) of MCM-48.[35] The N_2 adsorption-desorption behaviour and pore size distribution calculated from nonlocal density functional theory (NLDFT) method[40] are shown in Fig. 1 (c, d). A narrow pore size distribution with average size of 3.5 nm can be observed in Fig. 1 (d).

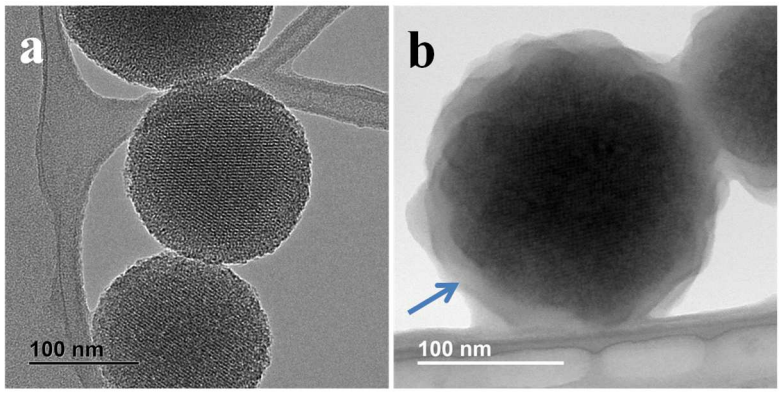

Figure 2. TEM image of MSNs (a) and MSNs-BTA@PDA (b). Arrow indicates PDA layer.

TEM analysis was performed in order to observe the nanoparticle inner structure before and after encapsulation. It can be seen from Fig. 2 (a) that the well-ordered pores are extending over the whole structure of MSNs. After the encapsulation and PDA surface decoration, the diameter of MSNs-BTA@PDA is ~10 % bigger than that of initial MSNs (Fig. 2 (b)). A rough PDA layer can be clearly seen from the surface of MSNs-BTA@PDA.

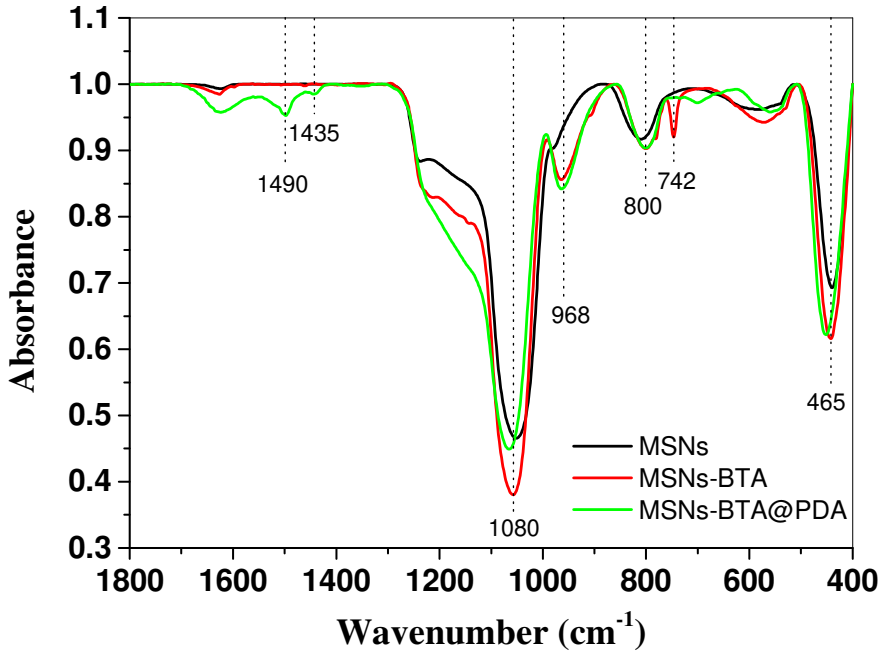

Figure 3. ATR-FTIR spectra of MSNs (black), MSNs-BTA (red), and MSNs-BTA@PDA (green).

Figure 3 shows the ATR-FTIR spectra of MSNs, MSNs-BTA, and MSNs-BTA@PDA samples. The absorption peaks at 465 cm^{-1}, 800 cm^{-1}, and 1080 cm^{-1} correspond to Si-O-Si bending vibration, Si-O-Si symmetric stretching, and Si-O asymmetric vibration, respectively. All these peaks are characteristic for SiO_2.[39] There is an absorption peak at 742 cm^{-1} for MSNs-BTA, which represents the C-H in plane bending vibrations of BTA benzene ring.[41] Furthermore, the peaks at 1435 and 1490 cm^{-1} on MSNs-BTA@PDA samples could be assigned to the skeletal vibration of aromatic double bonds, which indicates the presence of PDA.[42]

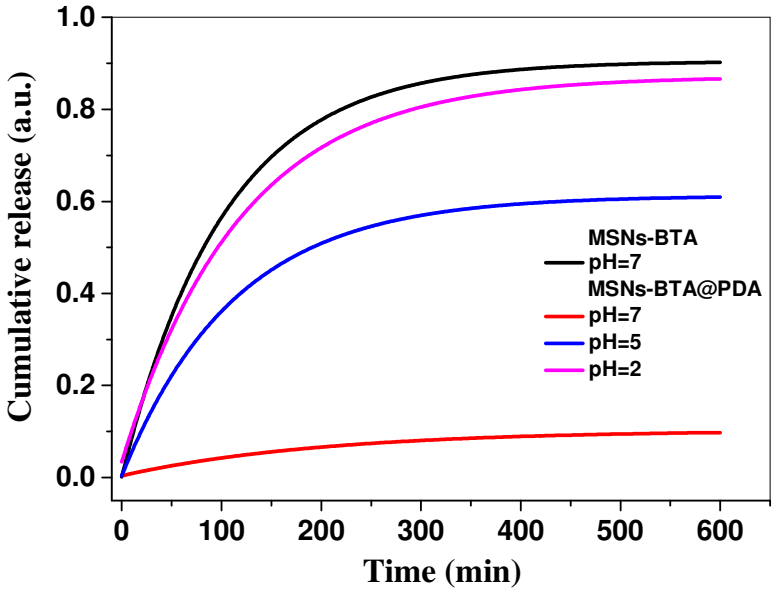

Figure 4. Release profile of BTA from the MSNs-BTA and MSNs-BTA@PDA nanocontainers at different pH values.

The release profiles of BTA from MSNs-BTA and MSNs-BTA@PDA nanocontainers are demonstrated in Figure 4. Fast release can be observed from the MSNs-BTA nanocontainers even at pH 7 (black line). Without polydopamine layer, nearly 60% of encapsulated BTA was released from the mesoporous nanocontainers within first 100 min. When we embedded these nanocontainers into the anticorrosion coatings, the BTA would start to leak from the first minute of immersion into paint formulation. It leads a large amount of inhibitor lost during the coating application and curing. In the case of MSNs-BTA@PDA, BTA release was suppressed by PDA at pH 7 (red line) as seen in Figure 4. At the same time, changing the pH value to acidic region results in of BTA release rate: 30 % of BTA at pH 5 and 50 % of BTA at pH 2 were released from the nanocontainers in first 100 min of exposure, respectively. At neutral pH, the PDA coating anchors functional ligands on the surface of MSNs via physical bonds (hydrogen bond or van der Waal's force) or chemical bonds (Michael addition or Schiff base reaction).[18] At low pH, the catechol groups of PDA, the inhibitor molecules, and the silica particles have the same charge, which leads to electrostatic repulsion forces inside the

nanocontainers. The PDA coatings were partially peeled off from the surface of MSNs in the acidic media.[19-20] Therefore, more BTA was released from the channels of the MSNs at low pH. Corrosion activity, which leads to local changes of pH, will trigger the release of BTA from MSNs-BTA@PDA nanocontainers.

Characterization of self-healing coatings.

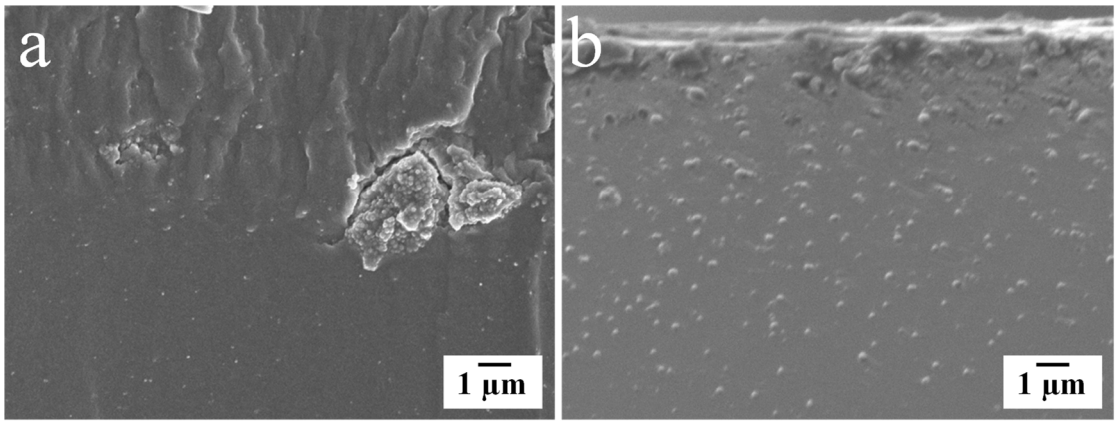

Figure 5. Ultramicrotomed SEM images of coating with MSNs (a) and MSNs-BTA@PDA (b).

Ultramicrotomed SEM analysis of coatings with nanocontainers was performed to study the dispersion of the nanocontainers inside the coating. It should be noted that the samples used for cross section observation were coated on the glass plate. So their thicknesses were different from the samples used for corrosion tests. Large amount of aggregated MSNs was observed in Fig. 5 (a), which indicates the poor dispersity of pure MSNs in the alkyd coating matrix. In contrast, homogeneous distribution of MSNs-BTA@PDA can be observed from Fig. 5 (b). It could be effect of –OH groups of PDA reacting with coating matrix thus enhancing nanocontainer dispersion in coatings. In addition, no bubbles or cracks can be seen in Fig. 5 (b), which indicates intact structure of the coating.

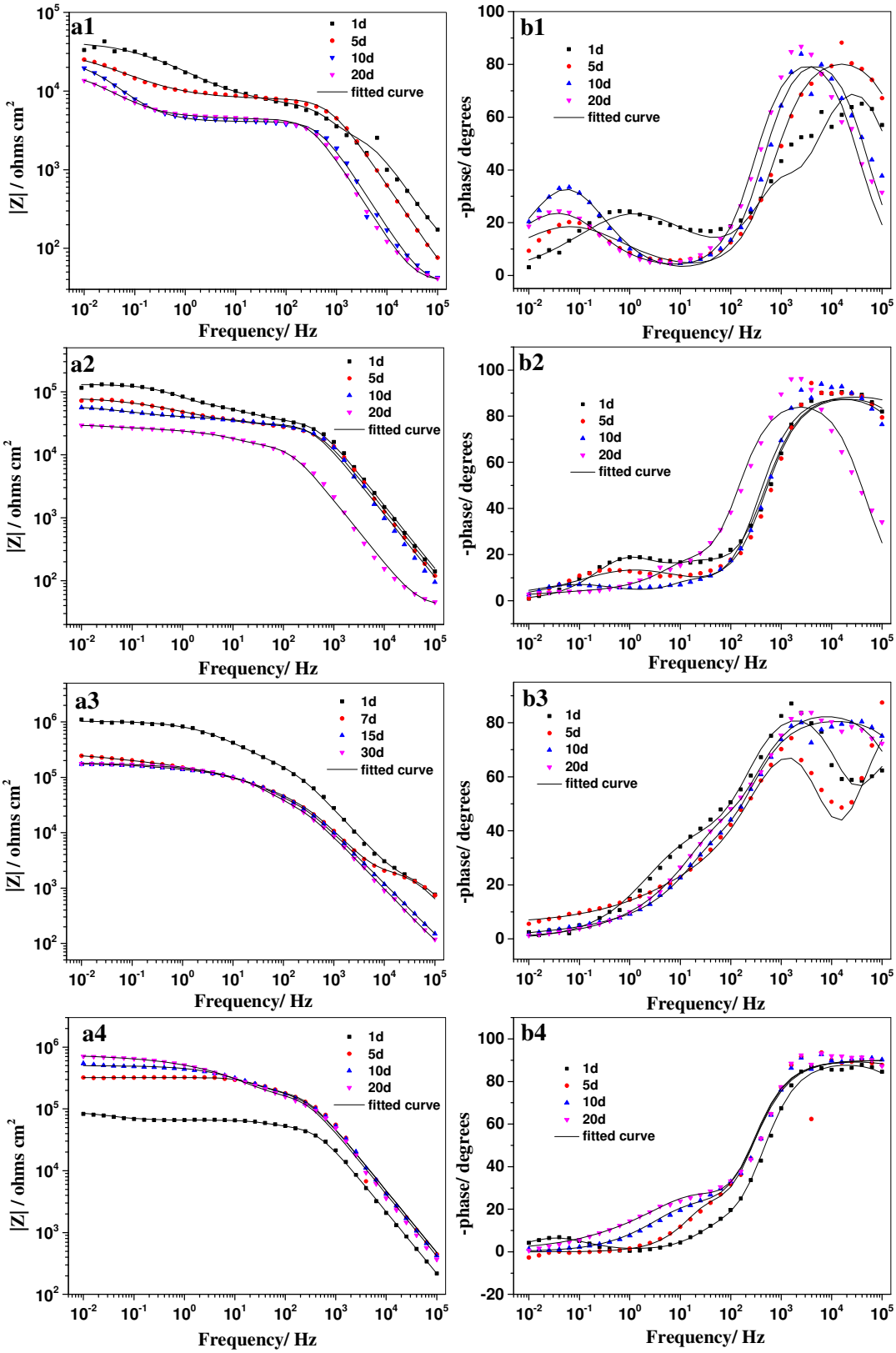

Figure 6. Bode plots of the scratched coatings during 20 days of immersion in 0.1 M NaCl: blank coating (a1, b1), coating with MSNs (a2, b2), with MSNs-BTA (a3, b3), and with MSNs-BTA@PDA (a4, b4).

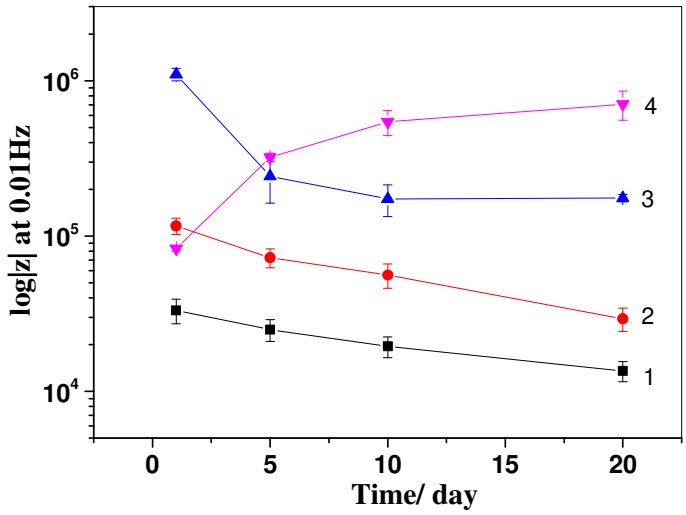

Figure 7. Impedance modulus |Z| measured at 0.01 Hz during immersion in 0.1 M NaCl for blank coating (1), coating with MSNs (2), with MSNs-BTA (3), and with MSNs-BTA@PDA (4).

Table 1. Values of important electrochemical parameters: the fitting model delivers a good fit quality (χ^2 < 0.01); all fitting were performed as a result of three parallel EIS experiments.

coatings	time (day)	R_s (Ω cm^2)	CPE_c (μF cm^{-2})	n --	R_c (kΩ cm^2)	CPE_{dl} (μF cm^{-2})	n --	R_{ct} (kΩ cm^2)
blank	1	23	0.16	0.90	7.39	22.90	0.83	36.59
	5	26	0.35	0.97	4.36	150.60	0.83	20.01
	10	40	0.87	0.94	3.95	246.30	0.88	19.63
	20	38	1.19	0.96	3.02	350.90	0.79	14.63
with MSN	1	8	0.10	0.97	34.85	6.88	0.83	43.82
	5	14	0.12	0.94	30.82	26.68	0.88	31.58
	10	16	0.14	0.90	27.99	28.15	0.85	23.40
	20	23	0.79	0.90	12.53	30.71	0.89	20.61
with MSN-BTA	1	37	0.02	0.84	54.96	0.04	0.88	187.60
	5	19	0.33	0.83	43.87	0.75	0.86	57.63
	10	21	0.93	0.95	22.21	2.68	0.79	11.77
	20	38	1.84	0.87	10.35	10.89	0.95	10.95
with MSN-BTA@PDA	1	22	0.07	0.91	51.97	5.42	0.91	23.63
	5	11	0.03	0.98	170.70	2.08	0.89	31.46
	10	24	0.04	0.94	182.50	0.04	0.96	250.80
	20	18	0.04	0.99	196.80	0.03	0.98	374.10

Artificial defects with 0.2 × 10 mm^2 size were made on the coatings in order to induce the corrosion process. EIS measurements were carried out to evaluate their self-healing

performance in 0.1 M NaCl. The impedance value of the coating with empty MSNs is a little higher than that of the blank coating. The Bode plots obtained from blank coating and coating with MSNs are quite similar (Fig. 6 (a1, a2)), which illustrates that the MSNs entrapped in the coating serves only as nanocontainers for corrosion inhibitor. With the increase of immersion time, the corrosive species gradually penetrate into the scratch of the coatings, resulting in the steady decrease of impedance modulus of blank coating and coating with empty MSNs (Fig. 6 (b1, b2)). Fig. 6 (a3) exhibits a highest impedance modulus (1.0×10^6 Ω cm^2) after 1 day immersion for the coating doped with MSNs-BTA. The fast release of the inhibitor could suppress the development of corrosion just after immersion of the sample. However, the |Z| shows a sharp drop from 1.0×10^6 Ω cm^2 to 2.4×10^5 Ω cm^2 after 5 days of immersion. The release profile (Fig. 4) proves that the leakage of BTA from the MSNs-BTA could happen in neutral solution. The BTA could directly release in the whole testing area. The direct doping of the coating with corrosion inhibitor could affect the adhesion between steel and coating or perform negative influence to the coating matrix,[8] which decrease corrosion protection of the coating. In the case of the coating with MSNs-BTA@PDA, the |Z| remains lower as compared with coating with MSNs and MSNs-BTA after 1 day immersion. It is probably due to the remaining hydroxyl group on the surface of MSNs-BTA@PDA, which can promote water penetration into the coating. However, the coating with MSNs-BTA@PDA shows a stable resistance increase on a long term from 8.3×10^4 Ω cm^2 to 7.0×10^5 Ω cm^2 during 20 immersion days (Fig. 6 (a4)). Such a self-healing action was not observed for other investigated coatings. The on-demand release of BTA from the nanocontainers provides durable protection of the scratched area. Fig. 7 shows the electrochemical impedance data at 0.01 Hz during 20 days immersion, which reflects the overall corrosion resistance of coatings.

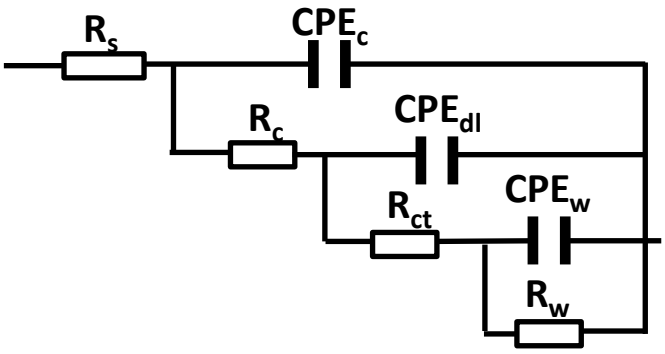

Figure 8. Electrical equivalent circuit used to fit the impedance data: R_s is solution resistance, R_c is coating resistance, CPE_c is constant phase element of coating capacitance, R_{ct} is charge transfer resistance, CPE_{dl} stands for constant phase element of double layer capacitance, R_w and CPE_w were used to describe the mass transport .

Electrical equivalent circuit shown in Fig. 8 was used to analyze the impedance data. The model circuit demonstrated an excellent fitting quality as shown in Fig. 6. The obtained fitting parameters for the coating response are depicted in Table 1. The value of CPE_{dl} (double layer capacitance) for coatings with MSNs-BTA@PDA is lower than for other coatings, which reflects a good adhesion of the coating to the metal.

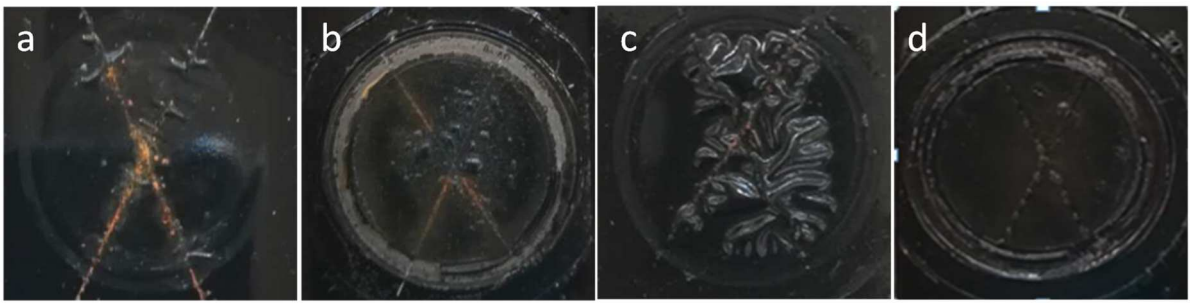

Figure 9. Images of blank coating (a), coatings with MSNs (b), MSNs-BTA (c), and MSNs-BTA@PDA (d) after 20 days of immersion in 0.1 M NaCl solution.

Figure 9 shows the optical images of coatings after 20 days of immersion in 0.1 M NaCl solution. Massive corrosion products are observed in the scratched area of the coatings in Fig. 9 (a, b) for blank coating and coating with MSNs, which indicates their poor corrosion resistance. Lower amount of rust is found on the image of coating with MSNs-BTA (Fig. 9(c)). However, a large area of coating was delaminated from the metal substrate showing weak adhesion between coating and substrate. This is in accordance with the impedance results,

which suggests that the fast release of BTA decreases the adhesion between coating and steel substrate. In the case of coating with MSNs-BTA@PDA (Fig. 9 (d)), no corrosion products and no delamination were found in the whole immersion area. Salt spray tests were taken to achieve a better knowledge of the failure process. Images of mild steel and mild steel coated with all kinds of coatings before and after 288 h of salt spray tests are shown in Figure 10. More detailed salt spray test images at different time periods are shown in Figure S2. Better performances were obtained for the mild steel coated with alkyd paint with MSNs-BTA@PDA, which proves their self-healing functionality and better barrier properties. Although all the coatings failed after 288 h salt spray test, the mild steel coated with alkyd paint with MSNs-BTA@PDA shows less rust on the surface than other samples. The coating with MSNs started to blister and bubble after 24 h while the coating with MSNs-BTA@PDA started to blister and bubble after 72 h (see Figure S2). These results confirm the improved anti-corrosion properties of coating with MSNs-BTA@PDA nanocontainers.

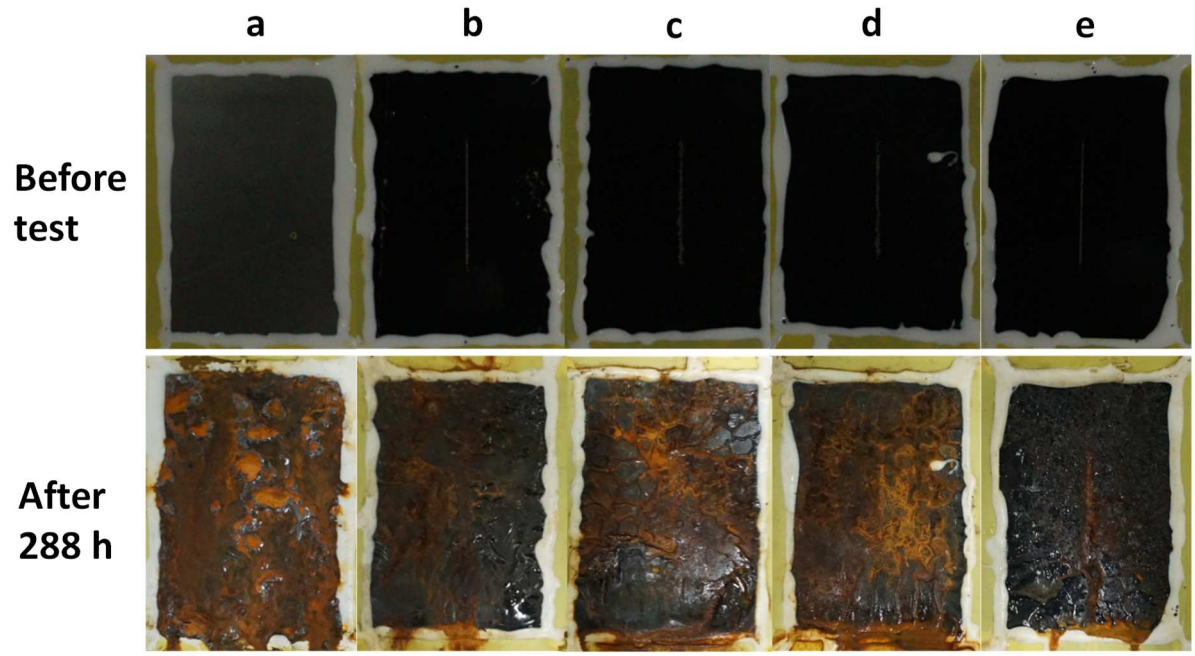

Figure 10. Images of mild steel (a), blank coating (b), coatings with MSNs (c), MSNs-BTA (d), and MSNs-BTA@PDA (e) before and after 288 h of salt spray test.

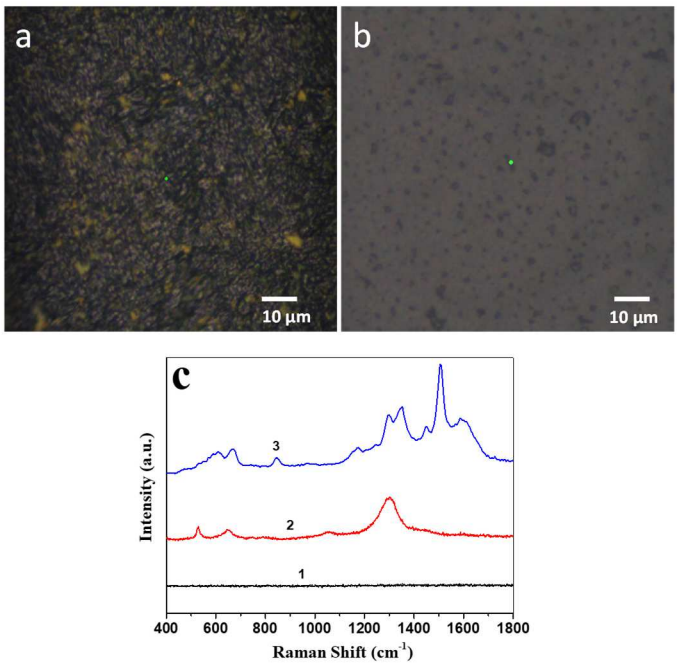

Figure 11. Blank coating (a) and coating with MSNs-BTA@PDA nanocontainers (b) images taken by confocal Raman microscope after 20 days of immersion in 0.1 M NaCl; (c) Raman spectra of (1) mild steel before immersion, (2) mild steel after removal of the blank coating or coating with MSNs-BTA@PDA (3) after 20 days of immersion.

Figure 11 (a, b) shows confocal Raman the images of coatings after immersion for 20 days in 0.1 M NaCl. These images were taken by Raman microscope in order to observe the rust and complex more clearly. Rust (yellow colour) could be found in the unscratched area of blank coating (Fig. 11 (a)). Fig. 11 (b) shows some dark complexes inside the micropores of the coating with MSNs-BTA@PDA nanocontainers. To eliminate the signal interference of the coating matrix, the Raman spectra were performed directly on the mild steel substrate after careful removal of the coatings. No obvious peak can be seen from the blank sample (line 1 in Fig. 11 (c)), which indicates that no rust or oxide were formed on the surface of mild steel before immersion. Three peaks are observed at 532, 654, and 1300 cm^{-1} for the steel coated with blank coating after immersion (line 2 in Fig. 11 (c)), which are assigned to γ-FeOOH and α-Fe_2O_3.[43] The Raman spectrum of mild steel (line 3 in Fig. 11 (c)) beneath the self-healing coatings with MSNs-BTA@PDA is different from blank sample. Raman peaks between 470 and 670 cm^{-1} are chelate peaks between Fe^{3+} and PDA catechol group.[44-45] The other peaks at

812, 1272, 1330, 1483 and 1566 cm^{-1} are characteristic Raman vibrations of dopamine.[46] Raman spectra confirm the existence of complexes between steel substrate and PDA.

CONCLUSIONS

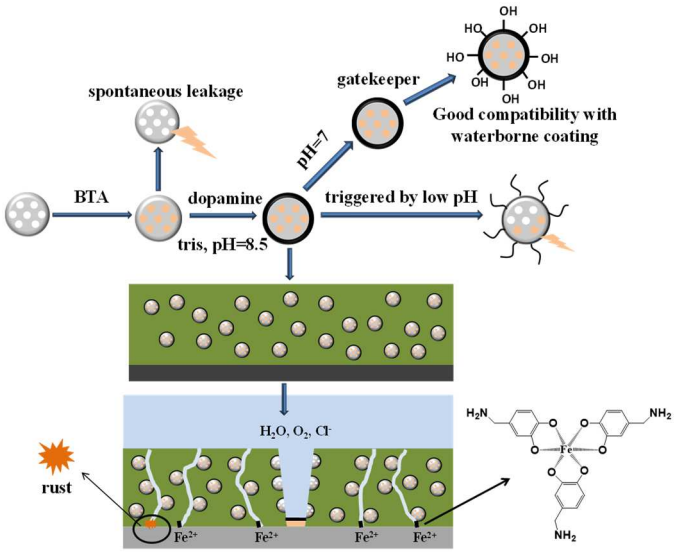

Figure 12. The self-healing mechism of the mussel-inspired coatings. In scratched area, the released BTA creates a protective film on the surface of mild steel. The detached dopamine also forms coordination complexes, which provide additional protective effect for the mild steel.

In this paper, we designed a novel pH-sensitive inhibitor release system by using the polydopamine (PDA) as the gatekeeper for mesoporous silica nanocontainers (MSNs) of 90-170 nm size loaded with corrosion inhibitor benzotriazole (BTA). TEM and ATR-FTIR results confirmed the presence of PDA layer on the surface of nanoparticles. Release profiles under different pH confirm the pH responsive kinetics of MSNs-BTA@PDA nanocontainers. The encapsulated inhibitor was trapped inside the MSNs in neutral pH while rapidly released in acidic environment. We embedded MSNs-BTA@PDA nanocontainers into a water-based alkyd coating and painted it on the surface of mild steel (Figure 12). Stable increase of the impedance modulus at 0.01 Hz for coatings with 2 wt% of incorporated MSN-BTA@PDA during 20 days of immersion in 0.1 M NaCl solution demonstrated high corrosion resistance and self-healing effect. Raman spectra confirmed the existence of complexes between steel substrate and PDA component of MSNs-BTA@PDA nanocontainers. PDA makes complex with corrosion products in the micropores of water-borne coatings as shown in Fig. 12. PDA

layer not only controls the release of inhibitor but also serves as a chelate agent to form protective complexes with corrosion products. Furthermore, the outer surface of MSN-BTA@PDA is functionalized with -OH groups from PDA for better dispersion in water-borne coatings. We hope that our work will inspire other researchers working in the field of corrosion protection to explore multifunctional properties of dopamine as a gatekeeper for other types of core-shell nanocontainers.

ASSOCIATED CONTENT

Supporting Information

Schematic diagram of the cell for electrochemical impedance spectroscopy and images of salt spray tests.

AUTHOR INFORMATION

Corresponding Author

*E-mail: D.Shchukin@liverpool.ac.uk (D.S.).

ORCID

Bei Qian: 0000-0002-2522-4647

Zhaoliang Zheng: 0000-0001-6741-6148

Marios Michailids: 0000-0001-8845-2375

Nicole Fleck: 0000-0001-7800-056X

Matthew Bilton: 0000-0002-0475-2942

Guoliang Li: 0000-0002-8054-6905

Dmitry Shchukin: 0000-0002-2936-804X

Notes

Any additional relevant notes should be placed here.

ACKNOWLEDGMENT

Dr. B.Q. was supported by the Shandong Provincial Government Scholarship (China) to visit the University of Liverpool. The work was financially supported by Research Foundation for Distinguished Scholars of Qingdao Agricultural University (663-1115017), Shandong Province Natural Science Foundation, China (ZR2017BD038, ZR2016DM21), and Natural Science Foundation of China (51801110), ERC Projects Enercapsule (647969) and Enerpaint (767173).

REFERENCES

(1) Hua, Z.; Hongxia, W.; Haitao, N.; Yan, Z.; Zhiguang, X.; Tong, L., A Waterborne Coating System for Preparing Robust, Self-healing, Superamphiphobic Surfaces. *Adv. Funct. Mater.* **2017,** *27*, 1604261.

(2) Li, J.; Feng, Q.; Cui, J.; Yuan, Q.; Qiu, H.; Gao, S.; Yang, J., Self-assembled Graphene Oxide Microcapsules in Pickering Emulsions for Self-healing Waterborne Polyurethane Coatings. *Compos. Sci. Technol.* **2017,** *151*, 282-290.

(3) Wan, T.; Chen, D., Synthesis and Properties of Self-healing Waterborne Polyurethanes Containing Disulfide Bonds in the Main Chain. *Journal of Materials Science* **2017,** *52*, 197-207.

(4) Shchukin, D. G.; Zheludkevich, M.; Yasakau, K.; Lamaka, S.; Ferreira, M. G. S.; Möhwald H., Layer-by-Layer Assembled Nanocontainers for Self-Healing Corrosion Protection. *Adv. Mater.* **2006,** *18*, 1672-1678.

(5) Shchukin, D. G.; Grigoriev, D. O.; Mohwald, H., Application of Smart Organic Nanocontainers in Feedback Active Coatings. *Soft Matter* **2010,** *6*, 720-725.

(6) Hollamby, M. J.; Fix, D.; Dönch, I.; Borisova, D.; Möhwald, H.; Shchukin, D., Hybrid Polyester Coating Incorporating Functionalized Mesoporous Carriers for the Holistic Protection of Steel Surfaces. *Adv. Mater.* **2011,** *23*, 1361-1365.

(7) Zheng, Z.; Schenderlein, M.; Huang, X.; Brownbill, N. J.; Blanc, F.; Shchukin, D., Influence of Functionalization of Nanocontainers on Self-Healing Anticorrosive Coatings. *ACS Appl. Mat. Interfaces* **2015,** *7*, 22756-22766.

(8) Borisova, D.; Möhwald, H.; Shchukin, D. G., Mesoporous Silica Nanoparticles for Active Corrosion Protection. *ACS Nano* **2011,** *5*, 1939-1946.

(9) Zheng, Z.; Huang, X.; Schenderlein, M.; Borisova, D.; Cao, R.; Möhwald, H.; Shchukin, D.; Self-Healing and Antifouling Multifunctional Coatings Based on pH and Sulfide Ion Sensitive Nanocontainers. *Adv. Funct. Mater.* **2013,** *23*, 3307-3314.

(10) Zheng, Z.; Huang, X.; Schenderlein, M.; Moehwald, H.; Xu, G. K.; Shchukin, D. G., Bioinspired Nanovalves With Selective Permeability and pH Sensitivity. *Nanoscale* **2015,** *7*, 2409-2416.

(11) Zheng, Z.; Huang, X.; Shchukin, D., A Cost-effective pH-sensitive Release System for Water Source pH Detection. *Chem. Commun.* **2014,** *50*, 13936-13939.

(12) Chen, T.; Fu, J. J., An Intelligent Anticorrosion Coating Based on pH-responsive Supramolecular Nanocontainers. *Nanotechnology* **2012,** *23, 505705*.

(13) Chen, T.; Fu, J. J., pH-responsive Nanovalves Based on Hollow Mesoporous Silica Spheres for Controlled Release of Corrosion Inhibitor. *Nanotechnology* **2012,** *23, 235605*.

(14) Ding, C.; Xu, J.; Tong, L.; Gong, G.; Jiang, W.; Fu, J., Design and Fabrication of a Novel Stimulus-Feedback Anticorrosion Coating Featured by Rapid Self-Healing Functionality for the Protection of Magnesium Alloy. *ACS Appl. Mat. Interfaces* **2017,** *9*, 21034-21047.

(15) Fu, J.; Chen, T.; Wang, M.; Yang, N.; Li, S.; Wang, Y.; Liu, X., Acid and Alkaline Dual Stimuli-Responsive Mechanized Hollow Mesoporous Silica Nanoparticles as Smart Nanocontainers for Intelligent Anticorrosion Coatings. *ACS Nano* **2013,** *7*, 11397-11408.

(16) Ding, C.; Tong, L.; Fu, J., Quadruple Stimuli-Responsive Mechanized Silica Nanoparticles: A Promising Multifunctional Nanomaterial for Diverse Applications. *Chemistry – A European Journal* 2017, *23*, 15041-15045.

(17) Ryu, J. H.; Messersmith, P. B.; Lee, H., Polydopamine Surface Chemistry: A Decade of Discovery. *ACS Appl. Mat. Interfaces* **2018,** *10*, 7523-7540.

(18) Lee, H.; Dellatore, S. M.; Miller, W. M.; Messersmith, P. B., Mussel-Inspired Surface Chemistry for Multifunctional Coatings. *Science* **2007,** *318*, 426-430.

(19) Chang, D.; Gao, Y.; Wang, L.; Liu, G.; Chen, Y.; Wang, T.; Tao, W.; Mei, L.; Huang, L.; Zeng, X., Polydopamine-based Surface Modification of Mesoporous Silica Nanoparticles as pH-sensitive Drug Delivery Vehicles for Cancer Therapy. *J. Colloid Interface Sci.* **2016,** *463*, 279-287.

(20) Zeng, X.; Tao, W.; Liu, G.; Mei, L., Polydopamine-based Surface Modification of Copolymeric Nanoparticles as a Targeted Drug Delivery System for Cancer Therapy. *J. Controlled Release* **2017,** *259*, e150-e151.

(21) Xia, N. N.; Xiong, X. M.; Wang, J.; Rong, M. Z.; Zhang, M. Q., A Seawater Triggered Dynamic Coordinate Bond and its Application for Underwater Self-healing and Reclaiming of Lipophilic Polymer. *Chemical Science* **2016,** *7*, 2736-2742.

(22) Kim, S.; Yoo, H. Y.; Huang, J.; Lee, Y.; Park, S.; Park, Y.; Jin, S.; Jung, Y. M.; Zeng, H.; Hwang, D. S.; Jho, Y., Salt Triggers the Simple Coacervation of an Underwater Adhesive When Cations Meet Aromatic π Electrons in Seawater. *ACS Nano* **2017,** *11*, 6764-6772.

(23) Chen, S.; Chen, Y.; Lei, Y.; Yin, Y., Novel Strategy in Enhancing Stability and Corrosion Resistance for Hydrophobic Functional Films on Copper Surfaces. *Electrochem. Commun.* **2009,** *11*, 1675-1679.

(24) Chen, Y.; Zhao, S.; Chen, M.; Zhang, W.; Mao, J.; Zhao, Y.; Maitz, M. F.; Huang, N.; Wan, G., Sandwiched Polydopamine (PDA) Layer for Titanium Dioxide (TiO_2) Coating on Magnesium to Enhance Corrosion Protection. *Corros. Sci.* **2015,** *96*, 67-73.

(25) Ghelichkhah, Z.; Sharifi-Asl, S.; Farhadi, K.; Banisaied, S.; Ahmadi, S.; Macdonald, D. D., L-cysteine/polydopamine Nanoparticle-coatings for Copper Corrosion Protection. *Corros. Sci.* **2015,** *91*, 129-139.

(26) Ou, J.; Wang, J.; Zhou, J.; Liu, S.; Yu, Y.; Pang, X.; Yang, S., Construction and Study on Corrosion Protective Property of Polydopamine-based 3-layer Organic Coatings on Aluminum Substrate. *Prog. Org. Coat.* **2010,** *68*, 244-247.

(27) Wang, C.; Shen, J.; Xie, F.; Duan, B.; Xie, X., A Versatile Dopamine-induced Intermediate Layer for Polyether Imides (PEI) Deposition on Magnesium to Render Robust and High Inhibition Performance. *Corros. Sci.* **2017,** *122*, 32-40.

(28) Wang, N.; Zhang, Y.; Chen, J.; Zhang, J.; Fang, Q., Dopamine Modified Metal-organic Frameworks on Anti-corrosion Properties of Waterborne Epoxy Coatings. *Prog. Org. Coat.* **2017,** *109*, 126-134.

(29) Wei, N.; Jiang, Y.; Ying, Y.; Guo, X.; Wu, Y.; Wen, Y.; Yang, H., Facile Construction of a Polydopamine-based Hydrophobic Surface for Protection of Metals Against Corrosion. *RSC Advances* **2017,** *7*, 11528-11536.

(30) Singer, F.; Schlesak, M.; Mebert, C.; Höhn, S.; Virtanen, S., Corrosion Properties of Polydopamine Coatings Formed in One-Step Immersion Process on Magnesium. *ACS Appl. Mat. Interfaces* 2015, *7*, 26758-26766.

(31) Zain, N. M.; Hussain, R.; Abdul Kadir, M. R., Quinone-rich Polydopamine Functionalization of Yttria Stabilized Zirconia for Apatite Biomineralization: The Effects of Coating Temperature. *Appl. Surf. Sci.* 2015, *346*, 317-328.

(32) Liang, L. G.; Matthias, S.; Yongjun, M.; Helmuth, M.; G., S. D., Monodisperse Polymeric Core–Shell Nanocontainers for Organic Self-Healing Anticorrosion Coatings. *Advanced Materials Interfaces* **2014,** *1*, 1300019.

(33) Cao, P. G.; Yao, J. L.; Zheng, J. W.; Gu, R. A.; Tian, Z. Q., Comparative Study of Inhibition Effects of Benzotriazole for Metals in Neutral Solutions As Observed with Surface-Enhanced Raman Spectroscopy. *Langmuir* **2002,** *18*, 100-104.

(34) Mennucci, M. M.; Banczek, E. P.; Rodrigues, P. R. P.; Costa, I., Evaluation of Benzotriazole as Corrosion Inhibitor for Carbon Steel in Simulated Pore Solution. *Cem. Concr. Compos.* **2009,** *31*, 418-424.

(35) Gomma, G. K., Corrosion Inhibition of Steel by Benzotriazole in Sulphuric Acid. *Mater. Chem. Phys.* **1998,** *55*, 235-240.

(36) Kim, T.-W.; Chung, P.-W.; Lin, V. S. Y., Facile Synthesis of Monodisperse Spherical MCM-48 Mesoporous Silica Nanoparticles with Controlled Particle Size. *Chem. Mater.* **2010,** *22*, 5093-5104.

(37) Schumacher, K.; Ravikovitch, P. I.; Du Chesne, A.; Neimark, A. V.; Unger, K. K., Characterization of MCM-48 Materials. *Langmuir* **2000,** *16*, 4648-4654.

(38) Schumacher, K.; Grün, M.; Unger, K. K., Novel Synthesis of Spherical MCM-48. *Microporous Mesoporous Mater.* **1999,** *27*, 201-206.

(39) Michailidis, M.; Sorzabal-Bellido, I.; Adamidou, E. A.; Diaz-Fernandez, Y. A.; Aveyard, J.; Wengier, R.; Grigoriev, D.; Raval, R.; Benayahu, Y.; D'Sa, R. A.; Shchukin, D., Modified Mesoporous Silica Nanoparticles with a Dual Synergetic Antibacterial Effect. *ACS Appl. Mat. Interfaces* **2017,** *9*, 38364-38372.

(40) Landers, J.; Gor, G. Y.; Neimark, A. V., Density Functional Theory Methods for Characterization of Porous Materials. *Colloids Surf., A* **2013,** *437*, 3-32.

(41) Barreto, L. S.; Tokumoto, M. S.; Guedes, I. C.; Melo, H. G. d.; Amado, F. D. R.; Capelossi, V. R., Evaluation of the Anticorrosion Performance of Peel Garlic Extract as Corrosion Inhibitor for ASTM 1020 Carbon Steel in Acidic Solution. *Matéria (Rio de Janeiro)* **2017,** *22*.

(42) Müller, M.; Keßler, B., Deposition from Dopamine Solutions at Ge Substrates: An in Situ ATR-FTIR Study. *Langmuir* **2011,** *27*, 12499-12505.

(43) de la Fuente, D.; Alcántara, J.; Chico, B.; Díaz, I.; Jiménez, J. A.; Morcillo, M., Characterisation of Rust Surfaces Formed on Mild Steel Exposed to Marine Atmospheres Using XRD and SEM/Micro-Raman Techniques. *Corros. Sci.* **2016,** *110*, 253-264.

(44) Holten-Andersen, N.; Harrington, M. J.; Birkedal, H.; Lee, B. P.; Messersmith, P. B.; Lee, K. Y. C.; Waite, J. H., pH-induced Metal-ligand Cross-links Inspired by Mussel Yield Self-healing Polymer Networks with Near-covalent Elastic Moduli. *PNAS* **2011,** *108*, 2651-2655.

(45) Kowalchyk, W. K.; Davis, K. L.; Morris, M. D., Surface-enhanced Resonance Raman Spectroscopy of Iron-dopamine Complexes. *Spectrochim. Acta, Part A* **1995,** *51*, 145-151.

(46) Ciubuc, J.; Bennet, K.; Qiu, C.; Alonzo, M.; Durrer, W.; Manciu, F., Raman Computational and Experimental Studies of Dopamine Detection. *Biosensors* **2017,** *7*, 43.

TOC Graphic

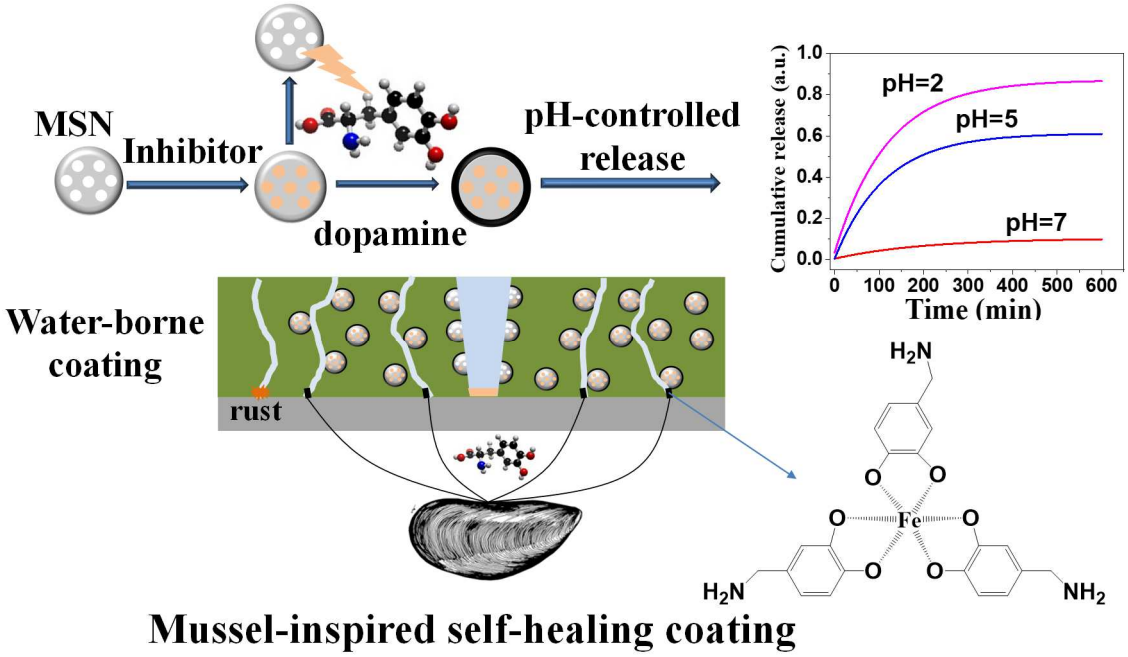

Mussel-inspired self-healing coating